Bulletin of the Chemical Society of Japan

Structures and Electronic Properties of Diisopropylaminoborane Substituted with Highly Electron-Rich π-Conjugated Systems and Their Oxidized States

Kohei Yoshida, Shuichi Suzuki,* Masatoshi Kozaki and Keiji Okada

Advance Publication on the web August 23, 2019
doi:10.1246/bcsj.20190199

Structures and Electronic Properties of Diisopropylaminoborane Substituted with Highly Electron-Rich π-Conjugated Systems and Their Oxidized States

Kohei Yoshida,[1] Shuichi Suzuki,*[1,2] Masatoshi Kozaki[1,3] and Keiji Okada[1,3]

[1]Graduate School of Science, Osaka City University, Sumiyoshi-ku, Osaka, Osaka 558-8585, Japan

[2]Graduate School of Engineering Science, Osaka University, Toyonaka, Osaka 560-8531, Japan

[3]Osaka City University Advanced Research Institute for Natural Science and Technology (OCARINA), Sumiyoshi-ku, Osaka, Osaka 558-8585, Japan

Shuichi Suzuki

Shuichi Suzuki graduated from Osaka University in 2001 and received his M.Sc. in 2003 and Ph.D. in 2006 under the supervision of Prof. Kazuhiro Nakasuji and Prof. Yasushi Morita. After receiving his Ph.D. degree, he joined Prof. Okada's research group at Osaka City University as an Assistant Professor. In 2010, he was promoted to Lecturer. In 2015, he moved to Osaka University as an Associate Professor. His current research interests focus on the developments of new functional materials based on unique molecular assemblies.

Abstract

We have designed and synthesized three kinds of diisopropylaminoboranes substituted with two electron-donating π-conjugated systems, **2a**: bis(phenothiazinyl) **2b**: bis(*N*-phenyldihydrophenazinyl), and **2c**: bis(phenoxazinyl) derivatives, and investigated their structures and electronic properties including those of oxidized species. The structural analyses of **2a–c** and **2a–c**$^{\bullet+}$ indicated that the π-electronic systems composed of boron and three nitrogen atoms showed unique structural deformation by one-electron-oxidation. The structures of the neutral compounds were almost C_2-symmetrical, indicating that the two donor π-electronic systems are almost identical. In contrast, the radical cationic compounds were not C_2-symmetrical structures because the charges of the radical cations were localized on one of the electron donors. In addition, the B–N bonds directly bound to the radical cations were elongated; also, perpendicular arrangements between the p-orbital of boron and π-conjugated orbitals of the radical cations were observed. We also succeeded in the observing the triplet state of **2b**$^{2(\bullet+)}$, which was categorized as a heteroatom analogue of the trimethylenemethane (TMM) π-electronic system, by means of electron-spin resonance (ESR) spectroscopy.

Keywords: Trimethylenemethane, Radical cation, Main group elements

1. Introduction

π-Conjugated compounds incorporating p-block elements other than carbon, nitrogen, and oxygen have been extensively studied for the exploration of their synthetic interests, for the elucidation of their electronic perturbations corresponding to related hydrocarbons, and for the development of unique electronic properties.[1–3] Of these research avenues, compounds possessing bonds composed of different kinds of typical elements have recently received great interests because of their unique molecular structures and electronic properties based on the polar character of the bonds.[3] Recently, we have focused on the B–N bond as a strongly polar bond due to its combinations of electron-deficient and electron-rich atoms. Compounds containing such bonds have been reported to show the fascinating photophysical and electronic properties derived from the polar characteristics of B–N bonds and their unique intra- and intermolecular interactions.[2h,i,k–3a,c,e] One of the interesting aspects of the amine moieties on B–N bonds is that they can be oxidized to form radical cationic bond which is a isoelectronic structure of the C=C radical cation,[4] the B–B radical anion,[5] and the C–B neutral radical.[6] We have investigated the electronic structure of the radical cationic species of tris(*N*-phenothiazinyl)borane (**1**),[7] and found (i) localization of the spin and charge on one of the phenothiazine moieties and (ii) elongation of the B–N bond directly bound to the phenothiazine radical cation. Additionally, when two-electron oxidized species of **1** has a planar structure, 2p orbitals of boron and three nitrogen atoms form a cross-conjugated system similar to trimethylenemethane (TMM) analogues. However, its congested structure prevents the planarization induced by the oxidation of the compound and generation of two-electron oxidized species. For further development of the present B–N π-electronic system and investigations of the B–N bonding properties, we designed a diisopropylaminoborane substituted with two phenothiazine (PTZ) units, **2a**, and its dihydrophenazine (DHP) and phenoxazine (PXZ) analogues, **2b** and **2c**, respectively (Figure 1), in which the aliphatic amine will provide the double bond characteristic for the B–N bond and stabilize the cationic species. Herein, we have synthesized and isolated the neutral and radical cationic species of **2a–c** and investigated their electronic structures. We have also succeeded in the generation of di(radical cationic) species **2b**$^{2(\bullet+)}$ which was an isoelectronic structure with the TMM diradical.

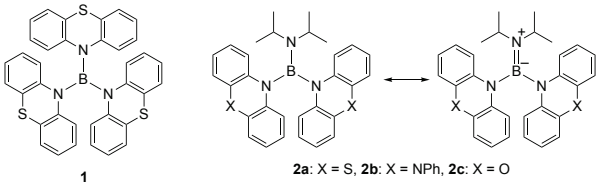

Figure 1. Chemical structures of **1** and **2a–c** with their resonance structures.

2. Experimental

General Information: Kanto Kagaku Silica gel 60 spherical was used for column chromatography. The progress of reactions was monitored using thin-layer chromatography using Merck TLC Aluminum oxide 60 F254 and Merck Silica gel 60 F254. Diisopropylaminodifluoroborane (iPr$_2$NBF$_2$)[9] and thianthrene radical cation tetrachlorogallate salt (**TH**$^{+}$•GaCl$_4^{-}$)[10] were prepared according to the literatures. Tris(4-bromophenyl)aminium hexafluoroantimonate (**TBPA**$^{\bullet+}$•SbF$_6^{-}$) was prepared from tris(4-bromophenyl)amine and silver hexafluoroantimonate according to literature with some modification.[11] 10-(4'-*tert*-Butylphenyl)-10*H*-phenothiazine (***t*-Bu-C$_6$H$_4$-PTZ**) was prepared from 10*H*-phenothiazine and 1-bromo-4-*tert*-butylbenzene by the cross-coupling reaction using Pd$_2$(dba)$_3$–*t*-BuOK in toluene. 5,10-Diphenyl-5,10-dihydrophenazine radical cation perchlorate (**DPP**$^{\bullet+}$•ClO$_4^{-}$)[12] and 10-phenyl-10*H*-phenoxazine radical cation hexafluorophosphate (**PXZ**$^{\bullet+}$•PF$_6^{-}$)[13] were prepared according to the literatures. Toluene, tetrahydrofuran (THF), and diethyl ether (Et$_2$O) were dried and distilled over sodium. Dichloromethane (CH$_2$Cl$_2$) and acetonitrile (CH$_3$CN) were dried and distilled over calcium hydride. The other chemicals were of commercial grade and used without further purification. ^{1}H and ^{13}C NMR spectra were recorded on a JEOL JNM-LA400 spectrometer. ESR spectra were recorded on a Bruker ELEXSYS E500 spectrometer. Melting points were measured using a Yanaco-MP-J3 apparatus and were not corrected. Infrared spectra were recorded using KBr pellets on a SHIMADZU FTIR-8700 spectrophotometer. UV/VIS/NIR absorption spectra were measured on SHIMADZU UV-2500. FAB-MS spectra were recorded on JMS-AX700 with NBA as a matrix. ESI-MS spectra were recorded on a Bruker micrOTOF II. Cyclic voltammogram measurements were carried out using ALS Electrochmical Analyzer Model 610A and recorded with a glassy carbon as a working electrode (WE), a Pt wire as a counter electrode (CE), and a saturated calomel electrode (SCE) as a reference electrode (RE) in dichloromethane containing 0.1 M *n*-butylammonium perchlorate (nBu$_4$N^{+}•ClO$_4^{-}$). The redox potentials were finally calibrated with the ferrocene/ferrocenium couple. UV/VIS/NIR absorption spectra during electrochemical oxidation were measured using an Ocean Optics HR4000 spectrometer, a 1-mm-width cell equipped with a fine mesh platinum as a WE, a Pt wire as a CE, and a SCE as a RE at suitable external potentials that could generate the radical cation species in dichloromethane in the presence of 0.1 M nBu$_4$NClO$_4$. X-ray data were collected by a Rigaku Saturn CCD system with graphite monochromated MoKα radiation. Elemental analyses were obtained from the Analytical Center in Osaka City University (using Fisons EA1108 and J-Science JM10).

***N*-(Di-10*H*-phenothiazin-10-ylboranyl)-*N*-(propan-2-yl)propan-2-amine (2a)**: 10*H*-Phenothiazine (**3a**) (1.40 g, 7.02 mmol) was dissolved in a mixture of toluene (60 mL) and THF (30 mL) under a nitrogen atmosphere. After cooling to 0 °C, a hexane solution of *n*-butyl lithium (1.65 M, 4.7 mL, 7.76 mmol) was added to the solution. Then, a toluene solution (5 mL) of iPr$_2$NBF$_2$ (524 mg, 3.52 mmol) was immediately added to the mixture. The mixture was stirred 22 h at room temperature, poured into water, and extracted with benzene. The organic layer was washed with water and a saturated aqueous NaCl solution, successively. The organic layer was dried over Na$_2$SO$_4$, filtered, and then concentrated under reduced pressure. The residue was purified by silica gel column chromatography using hexane–CH$_2$Cl$_2$ (4:1 v/v) as an eluent, to afford **2a** as a colorless solid (662 mg, 37%). Single crystals suitable for X-ray crystal analysis were obtained by recrystallization from CH$_2$Cl$_2$–ethanol. **2a**: C$_{30}$H$_{30}$BN$_3$S$_2$; colorless solid; MW 507.52; mp 231–232 °C; ^{1}H NMR (400 MHz, Acetone-d_6) δ (ppm) 7.22 (d, J = 7.5 Hz, 4H), 7.10 (br, 4H), 7.05 (td, J = 7.5 and 1.3 Hz, 4H), 6.98 (td, J = 7.5 and 1.3 Hz, 4H), 3.66 (sept, J = 6.2 Hz, 2H), 0.95 (d, J = 6.2 Hz, 12H); ^{13}C NMR (100 MHz, Acetone-d_6) δ (ppm) 145.4, 128.3, 128.2, 127.6, 124.7, 122.2, 48.2, 22.6; IR (KBr) 3058, 2977, 2958, 2929, 2868, 1589, 1573, 1477, 1460, 1365, 1317, 1299, 1228, 1188, 1172, 1157, 1118, 1074, 1039, 1002, 968, 929, 910, 893, 864, 850, 804, 746, 727, 707, 682, 659, 628, 588 cm^{-1}; MS (FAB^{+}) *m/z* 507 [M^{+}]; Anal. Calcd. for C$_{30}$H$_{30}$BN$_3$S$_2$: C, 71.00; H, 5.96; N, 8.28, Found: C, 70.75; H, 6.04, N, 8.20. Crystallographic data: CCDC 1936899.

***N*-[Bis(10-phenylphenazin-5(10*H*)-yl)boranyl]-*N*-(propan-2-yl)propan-2-amine (2b)**: Phenazine (435 mg, 2.41 mmol) was dissolved in a mixture of toluene (15 mL) and THF (5 mL) under a nitrogen atmosphere. After cooling to 0 °C, a di-*n*-butyl ether solution of phenyllithium (1.9 M, 1.4 mL, 2.64 mmol) was added to the solution. Then, a toluene solution (5 mL) of iPr$_2$NBF$_2$ (180 mg, 1.21 mmol) was immediately added to the mixture. The mixture was stirred for 21 h at room temperature, poured into water, and extracted with benzene. The organic layer was washed with water and a saturated aqueous NaCl solution, successively. The organic layer was dried over Na$_2$SO$_4$, filtered, and then concentrated under reduced pressure. Hexane was added to the residue and the precipitate was collected by filtration, to give **2b** as a brown solid (316 mg, 42%). Single crystals suitable for X-ray crystal analysis were obtained by recrystallization from CH$_2$Cl$_2$–hexane. **2b**: C$_{42}$H$_{40}$BN$_5$; reddish purple prism; MW 625.61; mp 214 °C (decomp.); ^{1}H NMR (400 MHz, Acetone-d_6) δ (ppm) 7.72 (d, J = 7.4 Hz, 4H), 7.56 (d, J = 7.4 Hz, 2H), 7.44 (d, J = 7.4 Hz, 4H), 6.97 (d-like, J = 7.0 Hz, 4H), 6.69–6.62 (m, 8H), 6.07 (dd, J = 7.0 and 1.9 Hz, 4H), 3.85 (sept, J = 6.8 Hz, 2H), 1.05 (d, J = 6.8 Hz, 12H); ^{13}C NMR (100 MHz, Acetone-d_6) δ (ppm) 142.1, 141.3, 136.7, 131.8, 131.4, 129.0, 123.5, 122.6, 119.9, 114.7, 48.3, 23.0; IR (KBr) 3061, 2963, 2926, 1593, 1479, 1458, 1437, 1331, 1277, 1244, 1194, 1157, 1105, 1070, 1055, 740, 700, 669, 646, 631, 617 cm^{-1}; MS (FAB^{+}) *m/z* 625 [M^{+}]; Anal. Calcd. for C$_{42}$H$_{40}$BN$_5$: C, 80.63; H, 6.44; N, 11.19, Found: C, 80.53; H, 6.60, N, 10.81. Crystallographic data: CCDC 1936903.

***N*-(Di-10*H*-phenoxazin-10-ylboranyl)-*N*-(propan-2-yl)propan-2-amine (2c)**: 10*H*-Phenoxazine (534 mg, 2.88 mmol) was dissolved in a mixture of toluene (20 mL) and THF (10 mL) under a nitrogen atmosphere. After cooling to 0 °C, a hexane solution of *n*-butyllithium (1.6 M, 1.9 mL, 3.02 mmol) was added to the solution. Then, a toluene solution (5 mL) of iPr$_2$NBF$_2$ (215 mg, 1.44 mmol) was immediately added to the mixture. The mixture was stirred for 17 h at room temperature, poured into water, and extracted with benzene. The organic layer was washed with water and a saturated aqueous NaCl solution, successively. The organic layer was dried over Na$_2$SO$_4$, filtered, and then concentrated under reduced pressure. The residue was purified by silica gel column chromatography using hexane–CH$_2$Cl$_2$ (4:1 v/v) as an eluent, to afford **2c** as a colorless solid (457 mg, 67%). Single crystals suitable for X-ray crystal analysis were obtained by recrystallization from CH$_2$Cl$_2$–ethanol. **2c**: C$_{30}$H$_{30}$BN$_3$O$_2$; colorless solid; MW 475.39; mp 206–207 °C; ^{1}H NMR (400 MHz, Acetone-d_6) δ (ppm) 7.03 (dd, J = 7.7 and 1.6 Hz, 4H), 6.96–6.84 (m, 12H), 3.67 (sept, J = 6.7 Hz, 2H), 1.01 (d, J = 6.7 Hz, 12H); ^{13}C NMR (100 MHz, Acetone-d_6) δ (ppm) 149.5, 135.4, 125.0, 124.2, 119.9, 117.2, 48.5, 23.2; IR (KBr) 3034, 2968, 2930, 2872, 1618, 1591, 1479, 1443, 1387, 1369, 1313, 1254, 1205, 1186, 1150, 1130, 1103, 1042, 1005, 914, 853,

837, 762, 737 cm^{-1}; MS (FAB^+) *m/z* 475 [M^+]; Anal. Calcd. for $C_{30}H_{30}BN_3O_2$: C, 75.79; H, 6.36; N, 8.84, Found: C, 75.78; H, 6.52, N, 8.82. Crystallographic data: CCDC 1936908.

Synthesis of $2a^{\bullet+}$•$GaCl_4^-$: In a glove box filled with an argon, **2a** (38 mg, 0.0740 mmol) was dissolved in CH_2Cl_2 (25 mL). To this stirred solution was added a CH_3CN solution (25 mL) of $\mathbf{TH}^{\bullet+}$•$GaCl_4^-$ (31 mg, 0.0735 mmol). After 30 min, the solvent was evaporated under reduced pressure. The residue was dissolved in CH_2Cl_2 (2 mL) and then Et_2O (20 mL) was slowly added to the CH_2Cl_2 solution. The generated precipitate was collected by filtration, to give $\mathbf{2a}^{\bullet+}$•$GaCl_4^-$ as a dark red solid (37 mg, 69%). The crystalline solid was obtained by recrystallization from CH_2Cl_2–benzene. $\mathbf{2a}^{\bullet+}$•$GaCl_4^-$: $C_{30}H_{30}BN_3S_2$•$GaCl_4$; dark red solid; MW 719.06; mp 189 °C (decomp.); MS (FAB^+) *m/z* 507 [$C_{30}H_{30}BN_3S_2^+$], (FAB^-) *m/z* 211 [$GaCl_4^-$]; IR (KBr) 3068, 3038, 2968, 2931, 2873, 1531, 1481, 1454, 1386, 1371, 1352, 1294, 1276, 1249, 1220, 1186, 1163, 1136, 1112, 1097, 1070, 1058, 1031, 989, 908, 893, 850, 804, 754, 740, 717, 680, 659, 634, 609, 594 cm^{-1}; Anal. Calcd. for $C_{30}H_{30}BN_3S_2$•$GaCl_4$: C, 50.11; H, 4.21; N, 5.84. Found: C, 49.96; H, 4.25; N, 5.86; g = 2.0054. Crystallographic data: CCDC 1936901.

Synthesis of $2b^{\bullet+}$•$GaCl_4^-$: In a glove box filled with an argon, **2b** (61 mg, 0.0978 mmol) was dissolved in CH_2Cl_2 (20 mL). To this stirred solution was added a CH_3CN solution (20 mL) of $\mathbf{TH}^{\bullet+}$•$GaCl_4^-$ (41 mg, 0.0962 mmol). After 30 min, the solvent was evaporated under reduced pressure. The residue was dissolved in CH_2Cl_2 (2 mL) and then Et_2O (20 mL) was slowly added to the CH_2Cl_2 solution. The generated precipitate was collected by filtration, to give $\mathbf{2b}^{\bullet+}$•$GaCl_4^-$ as a green solid (59 mg, 71%). The crystalline solid was obtained by recrystallization from CH_2Cl_2–toluene. $\mathbf{2b}^{\bullet+}$•$GaCl_4^-$: $C_{42}H_{40}BN_5$•$GaCl_4$; green solid; MW 837.15; mp 211 °C (decomp.); MS (FAB^+) *m/z* 625 [$C_{42}H_{40}BN_5^+$], (FAB^-) *m/z* 211 [$GaCl_4^-$]; IR (KBr) 3063, 2978, 2930, 2878, 1591, 1549, 1507, 1489, 1472, 1447, 1387, 1373, 1352, 1340, 1317, 1269, 1188, 1161, 1138, 1119, 1092, 1072, 745, 700, 669, 646, 631, 611 cm^{-1}; Anal. Calcd. for $C_{42}H_{40}BN_5$•$GaCl_4$: C, 60.26; H, 4.82; N, 8.37. Found: C, 59.88; H, 4.91; N, 8.05; g = 2.0031. Crystallographic data: CCDC 1936906.

Synthesis of $2c^{\bullet+}$•SbF_6^-: In a glove box filled with an argon, **2c** (51 mg, 0.106 mmol) was dissolved in CH_2Cl_2 (15 mL). To this stirred solution was added a CH_2Cl_2 solution (15 mL) of $\mathbf{TBPA}^{\bullet+}$•SbF_6^- (76 mg, 0.105 mmol). After 10 min, the solvent was evaporated under reduced pressure. The residue was dissolved in CH_2Cl_2 (2 mL) and then Et_2O (20 mL) was slowly added to the CH_2Cl_2 solution. The generated precipitate was collected by filtration, to give $\mathbf{2c}^{\bullet+}$•SbF_6^- as a purple solid (56 mg, 75%). The crystalline solid was obtained by recrystallization from CH_2Cl_2–hexane. $\mathbf{2c}^{\bullet+}$•SbF_6^-: $C_{30}H_{30}BN_3O_2$•SbF_6; purple solid; MW 711.140; mp 232 °C (decomp.); MS (ESI^+) *m/z* 475 [$C_{30}H_{30}BN_3O_2^+$], (ESI^-) *m/z* 235 [SbF_6^-]; IR (KBr) 3275, 2967, 2836, 2722, 1637, 1591, 1569, 1515, 1492, 1476, 1407, 1288, 1269, 1197, 1139, 1082, 952, 835, 759, 663 cm^{-1}; Anal. Cald. for $C_{30}H_{30}BN_3O_2$•SbF_6•$(CH_2Cl_2)_{0.2}$: C, 49.82; H, 4.21; N, 5.77. Found: C, 49.75; H, 4.26; N, 5.76. Crystallographic data: CCDC 1936909.

3. Results and Discussion

Syntheses of 2a–c: The syntheses of **2a–c** are illustrated in Scheme 1. Phenothiazine (**3a**) was treated with *n*-butyllithium in toluene/THF followed by the addition of diisopropylaminodifluoroborane ($i$$Pr_2NBF_2$)[9] to give **2a** in a 37% yield as a colorless solid. Phenazine **3b** was converted to a lithiated *N*-phenyl-9,10*H*-dihydrophenazine by substitution with phenyllithium and subsequent addition of $i$$Pr_2NBF_2$ to give **2b** in a 42% yield as a brown solid. Compound **2c** was obtained from phenoxazine **3c** in a 67% yield as a colorless solid by the same method as the preparation of **2a**. Compounds **2a–c** were stable against air and moisture. In the solution state, four aromatic NMR signals assigned to the donor moieties were observed, which suggested that the donor molecules could be freely rotated. We also obtained crystals of these compounds suitable for X-ray crystal structure analysis by recrystallization from suitable solvents.

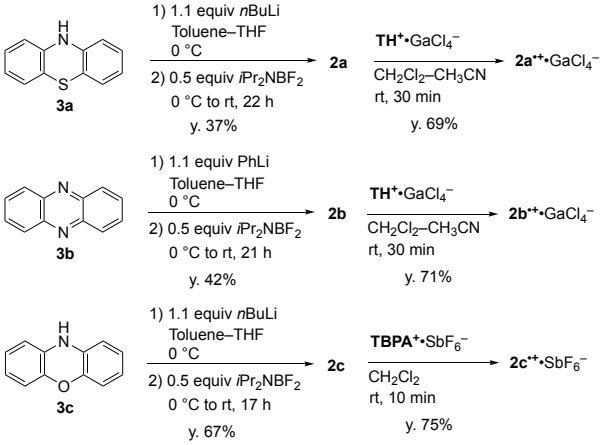

Scheme 1. Synthesis of **2a–c** and their corresponding cationic species.

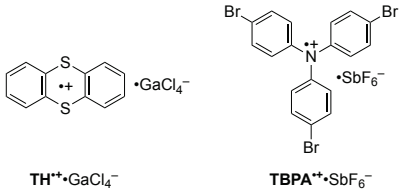

$\mathbf{TH}^{\bullet+}$•$GaCl_4^-$ $\mathbf{TBPA}^{\bullet+}$•SbF_6^-

Scheme 2. Chemical structures of oxidants used in the preparation of the radical cations.

Electrochemical properties of 2a–c: The cyclic voltammograms (CVs) of **2a–c** were measured to gain insight on their electrochemical properties (Figure 2, Table 1). Compounds **2a** and **2b** exhibited two reversible oxidation waves, while **1** exhibited one reversible and one irreversible oxidation waves at +0.20 V (vs Fc/Fc^+) and approximately +1.2 V,[7] respectively. The reversibility of the oxidation waves of **2a** and **2b** suggested that both the one- and two-electron oxidized species are stable within the time scale of the CV measurement; therefore, it would be possible to prepare the two-electron oxidized species. The CV of **2c** showed two oxidation waves with a residual wave at +0.12 V after the second oxidation processes, suggesting that the dication species are not stable (Figure S1). The large differences between the first and second oxidation waves for **2a–c** suggested that the molecular structures were largely changed by one-electron oxidation.

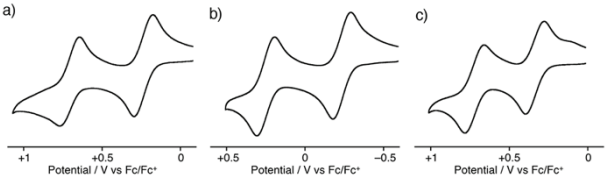

Figure 2. Cyclic voltammograms of (a) **2a**, (b) **2b**, and (c) **2c** in dichloromethane.

Table 1. Oxidation potentials of **2a–c** [a]

	$E_{1/2}^{ox1}$ / V	$E_{1/2}^{ox2}$ / V	$E_{1/2}^{ox2} - E_{1/2}^{ox1}$ / V
2a	+0.24	+0.71	0.47
2b	–0.24	+0.25	0.49
2c	+0.34	+0.72	0.38

[a] Conditions: 0.1 M *n*-$BuNClO_4$ in dichloromethane; V vs Fc/Fc^+ = 0 V (+0.48 V vs SCE); working electrode: glassy carbon; counter electrode: platinum; reference electrode: SCE; scan rate: 100 mV s^{-1}.

In order to investigate the stabilities of the oxidized species of **2a–c**, we monitored their UV/VIS/NIR spectra using a thin-layer cell during electrochemical oxidation through the application of the appropriate external potentials in dichloromethane solution containing 0.1 M tetra-*n*-butylammonium perchlorate (Figure 3). The spectrum of **2a** showed no absorption in visible region before oxidation (Figure 3a). During the electrochemical oxidation ($E_{applied}$ = +0.44 V vs Fc/Fc^+), new broad absorption bands were observed at λ_{max} = 514, 770, and 861 nm accompanied by an isosbestic point at 345 nm. The spectrum shape and molar absorption coefficients were similar to those of $\mathbf{1}^{\bullet+}$ [8] and the radical cation species of ***t*-Bu-C_6H_4-PTZ** (Figure S2), indicating that the radical cation species $\mathbf{2a}^{\bullet+}$ was quantitatively generated by the electrochemical oxidation. The spectrum also suggested that the spin and positive charge were localized on only one of the PTZ moieties, as was observed in the case for **1**.[7]

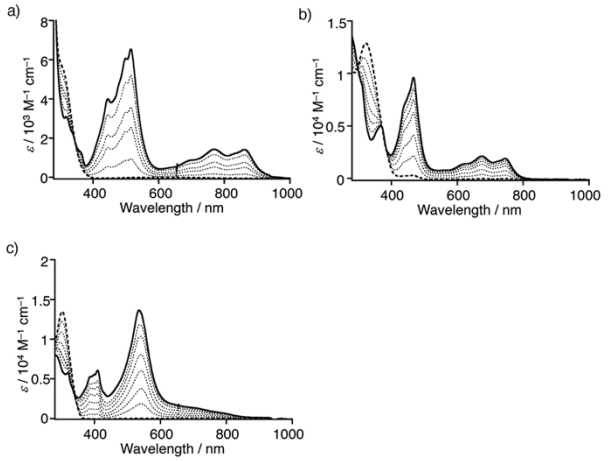

Figure 3. UV/VIS/NIR spectral changes during electrochemical oxidation of (a) **2a**, (b) **2b**, and (c) **2c**: The applied voltages for **2a**, **2b**, and **2c** were +0.44 V, –0.04 V, and +0.54 V (vs Fc/Fc^+), respectively. The dashed and solid lines show the spectra before and after oxidation, respectively. The dotted lines show intermediate states.

The overview of the absorption spectral change observed during the oxidation of **2b** was similar to that of **2a**. The spectrum of **2b** showed an absorption band at 323 nm along with a quite small absorption band at approximately 450 nm (Figure 3b). The latter absorption was attributed to the one-electron oxidation species of **2b** which was generated at the low levels by air oxidation due to its quite low oxidation potential. Absorption bands at λ_{max} = 466, 674, and 745 nm were increased with isosbestic points at 298 and 371 nm by the application of an external potential at –0.04 V, which was attributed to the absorptions of the DHP radical cation on the basis of the correlation to the spectrum shape of $\mathbf{DPP}^{\bullet+}\bullet ClO_4^-$ (Figure S3).[12] These results also indicated that the spin and charge are localized on one of the DHP moieties.

The UV/VIS/NIR spectrum of $\mathbf{2c}^{\bullet+}$ generated by an electrochemical reaction showed absorption bands at λ_{max} = 416, 535, and 722 nm (Figure 3c). Although the absorption maxima of the spectrum for $\mathbf{2c}^{\bullet+}$ were similar to that of $\mathbf{PXZ}^{\bullet+}\bullet PF_6^-$ (Figure S4),[13] the spectra shapes differed from one other. This observation suggested the instability of the $\mathbf{2c}^{\bullet+}$ species.

It is noted that degradation of the absorption bands of $\mathbf{2a–c}^{\bullet+}$ which lacked isosbestic points were observed by further electrochemical oxidation which was performed by applying the potential enough to generate the two-electron oxidized species of **2a–c**, suggesting the instability of $\mathbf{2a–c}^{2+}$ at room temperature.

Synthesis and characterization of the radical cations of 2a–c: The radical cations of **2a** and **2b** were obtained by chemical oxidations using a thianthrene radical cation tetrachlorogallate salt ($\mathbf{TH}^+\bullet GaCl_4^-$ in Scheme 2) as an oxidizing agent. The UV/VIS/NIR spectra of these radical cation salts in dichloromethane are quite similar to those of the electrochemically generated ones (Figures S5,S6). In addition, degradation of the UV/VIS/NIR absorption spectra were not observed under aerated conditions at room temperature, which indicated that these radical ions were quite stable.

To clarify the electronic spin structures of **2a** and **2b**, we measured their electron spin resonance (ESR) spectra in dichloromethane at room temperature (Figures 4,5). The ESR spectra could be reproduced by simulation with the aid of calculated hyperfine coupling constants (hfcs) using the *Gaussian 09* program (Figure S7).[14] The presence of two non-equivalent hfcs for the nitrogen nuclei bound to the boron atom indicates that the electron spin in **2a**/**2b** is localized on one of the PTZ or DHP moieties, respectively, consistent with the findings of the UV/VIS/NIR analysis. This localization was also suggested by the spin density distributions calculated with *Gaussian 09*.[14]

The tetrachlorogallate salt of $\mathbf{2c}^{\bullet+}$ could not be isolated. Therefore, the product from chemical oxidation with tris(4-bromophenyl)aminium hexafluoroantimonate ($\mathbf{TBPA}^{\bullet+}\bullet SbF_6^-$ in Scheme 2) was isolated as single crystals of $\mathbf{2c}^{\bullet+}\bullet SbF_6^-$ for further analysis. In contrast to the high stability of $\mathbf{2a}^{\bullet+}$ and $\mathbf{2b}^{\bullet+}$, $\mathbf{2c}^{\bullet+}$ decomposed in solution state. The UV/VIS/NIR spectrum of $\mathbf{2c}^{\bullet+}\bullet SbF_6^-$ in solution is different from that of the electrochemically generated radical ion of $\mathbf{2c}^{\bullet+}$ (Figure 6). Additionally, the shape of the spectrum changed depending on the exposure time to aerated conditions. The ESR spectral pattern was similar to that of $\mathbf{2a}^{\bullet+}$, although the spectrum of $\mathbf{2c}^{\bullet+}\bullet SbF_6^-$ in dichloromethane could not be reproduced by simulation.

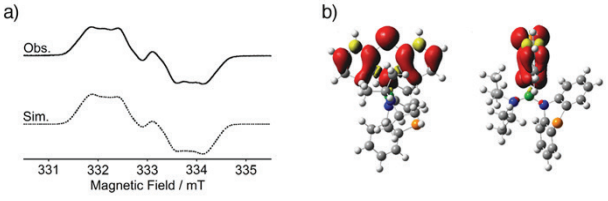

Figure 4. (a) Observed and simulated ESR spectra of $\mathbf{2a}^{\bullet+}\bullet GaCl_4^-$ in dichloromethane (g = 2.0054, ν_0 = 9.346556 MHz). (b) Top and side views of calculated spin density map of $\mathbf{2a}^{\bullet+}$. Red and yellow orbitals denoted the positive and negative spin densities, respectively. The calculations were carried out by the density functional theory with *Gaussian 09* at the UB3LYP/6-31G** level of theory using the coordinates extracted from the X-ray crystal structure.

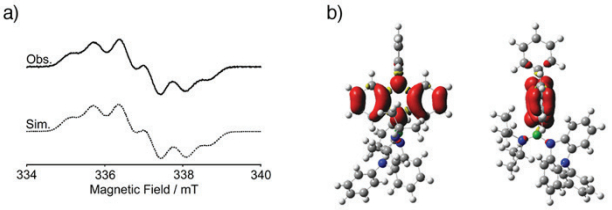

Figure 5. (a) Observed and simulated ESR spectra of **2b**$^{\bullet+}$•$GaCl_4^-$ in dichloromethane (g = 2.0031, ν_0 = 9.445195 MHz). (b) Top and side views of calculated spin density map of **2b**$^{\bullet+}$. Red and yellow orbitals denoted the positive and negative spin densities, respectively. The calculations were carried out by the density functional theory with *Gaussian 09* at the UB3LYP/6-31G** level of theory using the coordinates extracted from the X-ray crystal structure.

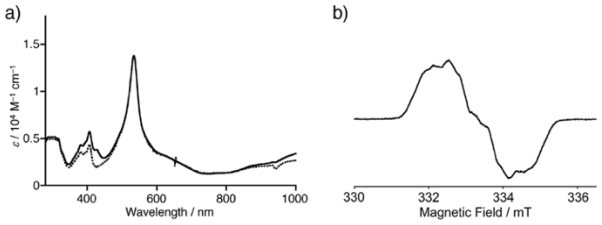

Figure 6. (a) UV/VIS/NIR spectra of **2c**$^{\bullet+}$•SbF_6^- in dichloromethane prepared from crystalline samples. The solid and dotted lines showed spectra as just prepared and after 30 min, respectively. (b) Observed ESR spectra of **2c**$^{\bullet+}$•SbF_6^- in dichloromethane.

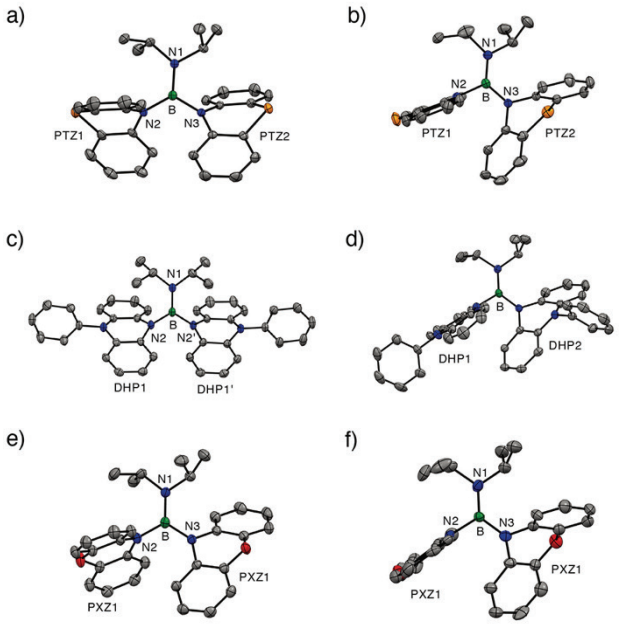

Figure 7. ORTEP views of (a) **2a**, (b) **2a**$^{\bullet+}$•$GaCl_4^-$, (c) **2b**, (d) **2b**$^{\bullet+}$•$GaCl_4^-$, (e) **2c**, and (f) **2c**$^{\bullet+}$•SbF_6^- (50% probabilities): Hydrogen atoms and counter ions are omitted for clarity. Carbon, nitrogen, oxygen, sulphur, and boron atoms are shown as gray, blue, red, orange, and green ellipsoids. For (c), the molecular structures of the DHP moieties and the isopropyl groups of **2b** were crystallographically equal because of a C_2-symmetric axis along the B–N1 bond. For (f), one of the structures of **2c**$^{\bullet+}$ is shown although two kinds of crystallographically independent units existed.

Crystal structures of 2a–c and their corresponding radical cations: Single crystals of **2a–c** and **2a–c**$^{\bullet+}$•X^- (X = $GaCl_4$ or SbF_6) suitable for X-ray crystal structure analysis were obtained by recrystallization from suitable solvents. The X-ray crystal structure analyses of these single crystals demonstrated the molecular conformational changes between the neutral and radical cationic species. The molecular structures are shown in Figure 7 (see also Figure 8 for discussions). Table S1 and S2 list the crystallographic data for **2a–c** and **2a–c**$^{\bullet+}$•X^- (X = $GaCl_4$ or SbF_6), respectively. Table S3 lists the bond lengths and dihedral angles surrounding the B–N π-electronic systems.

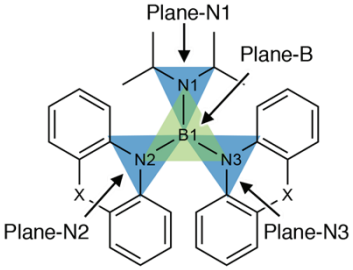

Figure 8. Specific names of atoms and plane for discussion of the crystal structures (N3 = N2 for **2b**).

The neutral compound **2a** exhibited a pseudo-C_2-symmetrical structure. The PTZ moieties in **2a** possessed folded structures along the N–S axis (butterfly structure).[7,13] The folded angles were found to be 139.6 and 138.2° for PTZ1 and PTZ2, respectively. The summation of the bond angles around N1, N2, and N3 were almost 360° (359.9, 359.6, and 359.9°, respectively), which suggested sp^2 hybridization of these atoms. Interestingly, the B–N1 bond (1.404(3) Å) was shorter than B–N2 and B–N3 (1.486(3), and 1.486(3) Å, respectively), which suggested that the B–N1 bond showed a slightly stronger double bond character. The dihedral angle between the plane defined by the atoms around B (Plane-B) and those around N1 (Plane-N1) was noticeably smaller than those of the corresponding dihedral angles between Plane B and around N2 and N3 (Plane-B/Plane-N1: 24.6°; Plane-B/Plane-N2: 56.1°; Plane-B/Plane-N3: 59.4°, respectively), indicating the slight double bond character of the B–N1 bond.

The overviews of the molecular structures of **2b** and **2c** in the crystalline states were similar to that of **2a** (Table S3). Compounds **2b** and **2c** exhibited C_2- and pseudo-C_2-symmetrical structures, respectively. The B–N1 bonds of both compounds were shorter than the other B–N bonds of the compounds. The dihedral angles defined atoms around B and those around N1 were quite small. These short bond lengths and small dihedral angles indicated that the B–N1 bonds of **2b** and **2c** had slight double bond character, based on the same reasoning as in the case of **2a**.

The structure of **2a**$^{\bullet+}$ was quite different from that of the corresponding neutral state. One of the phenothiazine moieties, PTZ1, was found to exhibit a planar structure with a folded angle of 176.4°, whereas the other (PTZ2) exhibited a folded structure with a folded angle of 131.0°. This observation suggested that (i) PTZ1 was in the radical cationic state and (ii) the radical cation was localized on the PTZ1 moiety.[13] The localization of the spin was consistent with the results of the UV/VIS/NIR and ESR spectra. Importantly, the bond length of B–N2 (1.547(4) Å) was significantly longer than those of the other B–N bonds (B–N1: 1.393(4) and B–N3: 1.440(3) Å, respectively). The B–N2 bond in the radical cationic state was longer than that in the neutral

state, while the other B–N bonds were shorter. In addition, the dihedral angle of Plane-B/Plane-N2 (86.0°) was much larger than those of Plane-B/Plane-N1 (26.1°) and Plane-B/Plane-N3 (25.7°), which indicated that the vacant p-orbital on B was almost perpendicular to the p-orbital on N2 but approximately parallel to those on N1 and N3.

Structural deformations similar to those between **2a** and **2a**$^{\bullet+}$ were also observed in the case of **2b**/**2b**$^{\bullet+}$ and **2c**/**2c**$^{\bullet+}$ (Table S3). The radical cationic molecules deformed from almost C_2-symmetric structures in their neutral states. The radical cationic donor moieties had planar structures and were linked by longer B–N2 bonds compared with lengths of the other B–N bonds of the structures. The B–N2 bonds were also longer than those in the neutral states. These observations suggested the localization of charge and spin on one of the donor moieties (in which the N2 atoms were presented). The analysis of the results of the dihedral angles related to the atoms around B and around N indicated that the vacant p-orbitals on B were almost perpendicular to the p-orbitals on N2 but approximately parallel to those on the other N.

Table 2. Wiberg bond indices of B–N bonds for **2a–c**/**2a–c**$^{\bullet+}$ [a]

	B–N1	B–N2	B–N3
2a	1.1026	0.7790	0.7796
2a$^{\bullet+}$	1.1158	0.6446	0.9488
2b	1.0367	0.8105	0.8105
2b$^{\bullet+}$	1.1015	0.6579	0.9573
2c	1.0824	0.7471	0.8462
2c$^{\bullet+}$ [b]	1.1698	0.6389	0.9339

[a] The calculations were carried out by the density functional theory with *Gaussian 09* at the UB3LYP/6-31G** level of theory using the coordinates extracted from the X-ray crystal structure. [b] The calculated results of one of the crystallographically independent molecules.

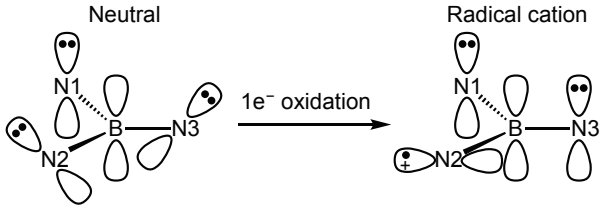

Scheme 2. Schematic representation of the electronic interactions between the vacant p-orbital on the B atom and the p-orbitals on the N atoms.

Wiberg bond indices of B–N bonds: Table 2 shows the Wiberg bond indices which were calculated by *Gaussian 09* on the basis of the crystal structures.[14,15] The indices of the B–N2 bonds in the oxidized states were smaller than those of the corresponding bonds in the neutral states. In contrast, the indices of the B–N1 and B–N3 bonds in the oxidized states were larger than those in the neutral states. In the oxidized states, positive charges were largely distributed on the N2, which induced the elongations of the B–N2 bonds and the large dihedral angles of the Plane-B/Plane-N2, attributed to unfavorable electronic interactions between the vacant p-orbital of B and the cationic p-orbital of N2 (Scheme 2). The B atoms in the radical cationic species became much more electron deficient than those in the neutral state because of the positively charged radical cation moiety. These effects led to the shorter lengths of the other B–N bonds compared to those in the neutral states and the higher coplanarities of Plane-B/Plane-N1 and Plane-B/Plane-N3 to the compensate for electron deficient environments on the B atoms by effective conjugations with the neutral nitrogen atoms. These electronic interactions were consistent with the Wiberg bond indices. The large difference between the first and second oxidation potentials of the donor moieties that were observed in the CVs induced by the structural deformations between the neutral and the radical cationic states. Notably, the Wiberg bond indices of the B–N1 bonds suggested the significant double bond character. The effective electron donating natures of N1 atoms enhanced the stability in the cationic states, making it possible to observe the two-electron oxidized species in the CVs. The B–N2 bond length in **2c**$^{\bullet+}$ was longer than the other B–N bonds, which induced the smallest Wiberg bond index of the B–N bonds of **2a–c**$^{\bullet+}$. This tendency of weak interactions in the B–N2 bond was presumed to be one of the reasons for the easy decomposition of **2c**$^{\bullet+}$.

Generation and detection of the di(radical cation) species of 2b: The results of the CV for **2b** prompted us to observe di(radical cation) species using **2b**. In an argon glove box, two equivalents of **TBPA**$^{\bullet+}$•SbF_6^- were added to the *n*-butyronitrile solution of **2b**. The solution was transferred to an ESR tube and its ESR spectrum was measured at 100 K (Figure 9a). Consequently, ESR signals attributed to randomly oriented triplet species were observed in the outer regions of the central broad signals for doublet impurities. Unfortunately, the spin-forbidden signal was not observed in a half-field region due to the low concentration of the di(radical cation) species. A spectral simulation yielded the following spin Hamiltonian parameters for the $S = 1$ state: $|D/hc| = 0.0176$ cm^{-1}, $|E/hc| \approx 0$ cm^{-1}, $g_{xx} = 2.0038$, $g_{yy} = 2.0038$, $g_{zz} = 2.0051$. The distance between the two spin-centers was calculated to be ~5.3 Å from the D value using the point-dipole approximation. This distance is comparable to that between the average centers of two dihydrophenadine π-electronic systems for the optimized structure from density functional theory (Figure 9b,c). The calculation also suggested that the di(radical cation) species of **2b** was found as a triplet in the ground state with a weak intramolecular exchange interaction ($2J/k_{B\_calcd} \sim +40$ K) (Table S4),[14,16] which is expected from the TMM π-electronic system. In the optimized structure of **2b**$^{2(\bullet+)}$, the π-planes of the dihydrophenazine radical cation moieties were almost perpendicular to the vacant p-orbital on B, which was correlated well with the case of the mono(radical cation)s.

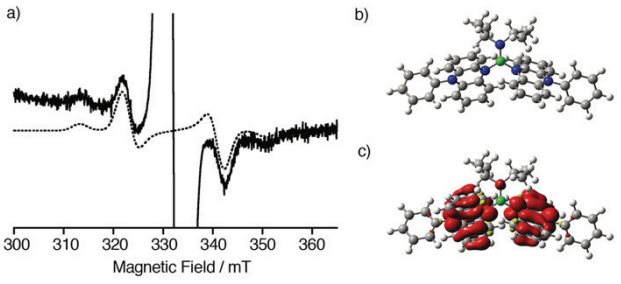

Figure 9. (a) Observed (solid line; in a frozen *n*-butyronitrile) and simulated (broken line) ESR spectra. (b) The optimized structure of **2b**$^{2(\bullet+)}$ in the triplet state and (c) spin densities calculated using *Gaussian 09* with UB3LYP/6-31G** level of theory. Red and yellow orbitals denoted the positive and negative spin densities, respectively.

4. Conclusion

We have designed and synthesized three kinds of diisopropylaminoborane substituted with two electron-donating π-conjugated moieties, **2a–c**, to investigate the detailed structures and electronic properties of unique B–N bond systems. The desired neutral compounds were obtained by generating the corresponding lithiated donor species followed by subsequent additions of iPr$_2$NBF$_2$. The radical cationic compounds **2a–c**$^{\bullet+}$ were also obtained by chemical oxidations using suitable oxidants. The neutral and radical cationic species, excluding for **2c**$^{\bullet+}$, had high stabilities under aerated conditions even in the solution states. The X-ray crystal structure analyses revealed unique structural deformations resulting from one-electron oxidations. The neutral compounds had almost C_2-symmetrical structures, whereas those in the radical cationic species were not C_2-symmetrical because the radical cations were localized on one of the electron donors. In the oxidized states, the nitrogen atom with radical cationic character induced the elongation of the B–N$^{\bullet+}$ bonds and the large dihedral angles of the Plane-B/Plane-N$^{\bullet+}$, explained by the unfavorable electronic interactions between the vacant p-orbital of the B atom and the cationic p-orbital of the N atom. Finally, we observed triplet ESR signals attributed to the two-electron oxidized species **2b**$^{2(\bullet+)}$, indicating that it has an isoelectronic structure with the TMM diradical systems.

Acknowledgement

This work was supported by Grant-in-Aid for Scientific Research (JSPS KAKENHI #Grant Numbers, JP15H00956 (K.O.) JP17K05790 (M.K. and K.O.) and JP26102005 (S.S), JP17K05783 (S.S)). We thank to Dr. Rika Tanaka for X-ray crystal structure analyses.

References

1. For example: (a) M. Hirai, N. Tanaka, M. Sakai, S. Yamaguchi, *Chem. Rev.* in press (DOI: 10.1021/acs.chemrev.8b00637). (b) P. G. Campbell, A. J. V. Marwitz, S.-Y. Liu, *Angew. Chem. Int. Ed.* **2012**, *51*, 6074. (c) A. Osuka, E. Tsurumaki, T. Tanaka, *Bull. Chem. Soc. Jpn.* **2011**, *84*, 679. (d) A. Fukazawa, S. Yamaguchi, *Chem. –Asian J.* **2009**, *4*, 1386. (e) M. Elbing, G. C. Bazan, *Angew. Chem. Int. Ed.* **2008**, *47*, 834. (f) T. Baumgartner, R. Réau, *Chem. Rev.* **2006**, *106*, 4681. (g) P. P. Power, *Chem. Rev.* **2003**, 103, 789. (h) J. Konu, T. Chivers, *Stable Radicals: Fundamentals and Applied Aspects of Odd-Electron Compounds,* ed. by R. G. Hicks, Wiley, Chichester, 2010, 381.
2. For example: (a) S. Yamaguchi, S. Akiyama, K. Tamao, *J. Am. Chem. Soc.* **2001**, *123*, 11372. (b) C. A. Jaska, D. J. H. Emslie, M. J. D. Bosdet, W. E. Piers, T. S. Sorensen, M. Parvez, *J. Am. Chem. Soc.* **2006**, *128*, 10885. (c) T. Agou, J. Kobayashi, Y. Kawashima, *Chem. –Eur. J.* **2007**, *13*, 8051. (d) P. Chen, R. A. Lalancette, F. Jäkle, *J. Am. Chem. Soc.* **2011**, *133*, 8802. (e) K. Okada, H. Inokawa, T. Sugawa, M. Oda, *J. Chem. Soc. Chem. Commun.* **1992**, 448. (f) K. Okada, T. Kawata, M. Oda, *J. Chem. Soc. Chem. Commun.* **1995**, 233. (g) H. Ito, T. Abe, K. Saigo, *Angew. Chem. Int. Ed.* **2011**, *50*, 7144. (h) T. Hatakeyama, S. Hashimoto, T. Oba, M. Nakamura, *J. Am. Chem. Soc.* **2012**, *134*, 19600. (i) M. Numano, N. Nagami, S. Nakatsuka, T, Katayama, K. Nakajima, S. Tatsumi, N. Yasuda, T. Hatakeyama, *Chem. –Eur. J.* **2016**, *22*, 11574. (j) K. Matsui, S. Oda, K. Yoshiura, K. Nakajima, N. Yasuda, T. Hatakeyama, *J. Am. Chem. Soc.* **2018**, *140*, 1195. (k) S. Nakatsuka, N. Yasuda, T. Hatakeyama, *J. Am. Chem. Soc.* **2018**, *140*, 13562.
3. (a) J. Yoshino, N. Kano, T. Kawashima, *Chem. Commun.* **2007**, 559. (b) A. Wakamiya, T. Taniguchi, S. Yamaguchi, *Angew. Chem. Int. Ed.* **2006**, *45*, 3170. (c) X.-Y. Wang, H.-R. Lin, T. Lei, D.-C. Yang, F.-D. Zhuang, J.-Y. Wang, S.-C. Yuan, J. Pei, *Angew. Chem. Int. Ed.* **2013**, 52, 3117. (d) T. Kushida, A. Shuto, M. Yoshio, T. Kato, S. Yamaguchi, *Angew. Chem. Int. Ed.* **2015**, *54*, 6922. (e) S. Hashimoto, T. Ikuta, K. Shiren, S. Nakatsuka, J. Ni, M. Nakamura, T. Hatakeyama, *Chem. Mater.* **2014**, *26*, 6265. (f) T. Hatakeyama, K. Shiren, K. Nakajima, S. Nomura, S. Nakatsuka, K. Kinoshita, J. Ni, Y. Ono, T. Ikura, *Adv. Mater.* **2016**, *28*, 2777.
4. R. Rathore, S. V. Lindeman, A. S. Kumar, J. K. Kochi, *J. Am. Chem. Soc.* **1998**, *120*, 6931.
5. H. Klusik, A. Berndt, *Angew. Chem. Int. Ed. Engl.* **1981**, *20*, 870.
6. (a) C.-W. Chiu, F. P. Gabbaï, *Angew. Chem. Int. Ed.* **2007**, *46*, 1723. (b) C.-W. Chiu, F. P. Gabbaï, *Angew. Chem. Int. Ed.* **2007**, *46*, 6878.
7. S. Suzuki, K. Yoshida, M. Kozaki, K. Okada, *Angew. Chem. Int. Ed.* **2013**, *52*, 2499.
8. For example, (a) W. T. Borden, *Diradicals*, ed. by W. T. Borden, John Wiley & Sons, New York, 1982, 1. (b) P. G. Wenthold, J. Hu, R. R. Squires, W. C. Lineberger, *J. Am. Chem. Soc.* **1996**, *118*, 475. (c) S. Suzuki, T. Furui, M. Kuratsu, M. Kozaki, D. Shiomi, K. Sato, T. Takui, K. Okada, *J. Am. Chem. Soc.* **2010**, *132*, 15908. (d) A. Konishi, Y. Okada, M. Nakano, K. Sugisaki, K. Sato, T. Takui, M. Yosuda, *J. Am. Chem. Soc.* **2017**, *139*, 15284.
9. A. Meller, U. Seebold, W. Maringgele, M. Noltemeyer, *Chem. Ber.* **1990**, 967.
10. M. Kuratsu, S. Suzuki, M. Kozaki, D. Shiomi, K. Sato, T. Takui, K. Okada, *Inorg. Chem.* **2007**, *46*, 10153.
11. S. Suzuki, K. Okada, *Organic Redox Systems*, ed. by T. Nishinaga, Wiley, New Jersey, 2016, chapter 8.
12. S. Suzuki, T. Takeda, M. Kuratsu, M. Kozaki, K. Sato, D. Shiomi, T. Takui, K. Okada, *Org. Lett.* **2009**, *11*, 2816.
13. A. Karimata, S. Suzuki, M. Kozaki, K. Okada, *RSC Adv.* **2017**, *7*, 56144.
14. *Gaussian 09*, Revision A.02, M. J. Frisch, G. W. Trucks, H. B. Schlegel, G. E. Scuseria, M. A. Robb, J. R. Cheeseman, G. Scalmani, V. Barone, B. Mennucci, G. A. Petersson, H. Nakatsuji, M. Caricato, X. Li, H. P. Hratchian, A. F. Izmaylov, J. Bloino, G. Zheng, J. L. Sonnenberg, M. Hada, M. Ehara, K. Toyota, R. Fukuda, J. Hasegawa, M. Ishida, T. Nakajima, Y. Honda, O. Kitao, H. Nakai, T. Vreven, J. A. Montgomery, Jr., J. E. Peralta, F. Ogliaro, M. Bearpark, J. J. Heyd, E. Brothers, K. N. Kudin, V. N. Staroverov, R. Kobayashi, J. Normand, K. Raghavachari, A. Rendell, J. C. Burant, S. S. Iyengar, J. Tomasi, M. Cossi, N. Rega, J. M. Millam, M. Klene, J. E. Knox, J. B. Cross, V. Bakken, C. Adamo, J. Jaramillo, R. Gomperts, R. E. Stratmann, O. Yazyev, A. J. Austin, R. Cammi, C. Pomelli, J. W. Ochterski, R. L. Martin, K. Morokuma, V. G. Zakrzewski, G. A. Voth, P. Salvador, J. J. Dannenberg, S. Dapprich, A. D. Daniels, Ö. Farkas, J. B. Foresman, J. V. Ortiz, J. Cioslowski, D. J. Fox, Gaussian, Inc., Wallingford CT, 2009.
15. (a) K. B. Wiberg, *Tetrahedron* **1968**, *24*, 1083. (b) T. Kar, J. G. Ángyán, A. B. Sannigrahi, *J. Phys. Chem. A* **2000**, *104*, 9953.
16. The exchange interaction was estimated by a compensation equation proposed by Yamaguchi and co-workers (Table S4). See, T. Kawakami, Y. Takano, Y. Kitagawa, Y. Yamashita, H. Fujita, *Int. J. Quantum Chem.* **2002**, *90*, 370.